PHOTONICS Research

Near-optimal intense and powerful terahertz source by optical rectification in lithium niobate crystal

L. Guiramand,[1] J. E. Nkeck,[1] X. Ropagnol,[1,2] T. Ozaki,[2] and F. Blanchard[1,*]

[1]Département de génie électrique, École de technologie supérieure, Montréal, Québec H3C 1K3, Canada
[2]Institut National de la Recherche Scientifique—Énergie Matériaux Télécommunications, Varennes, Québec J3X 1P7, Canada
*Corresponding author: francois.blanchard@etsmtl.ca

Received 20 April 2021; revised 15 November 2021; accepted 21 November 2021; posted 23 November 2021 (Doc. ID 428418); published 11 January 2022

Using a 400 μJ ytterbium laser combined with a novel pulse compression technique, we demonstrate a state-of-the-art terahertz (THz) source from the tilted-pulse front pumping scheme in lithium niobate at room temperature with record efficiency of 1.3% capable of generating 74 mW of average power and 400 kV/cm at focus. Key points of this demonstration include the use of a pump pulse duration of 280 fs in combination with a stair-step echelon mirror and an off-axis ellipsoidal mirror. This source has unmatched characteristics of generating intense and powerful THz pulses at the same time and remains highly scalable as compared to existing Ti:sapphire-based THz sources pumped in the millijoule range.

https://doi.org/10.1364/PRJ.428418

1. INTRODUCTION

Intense electromagnetic radiation in the terahertz (THz) frequency range has been used for various groundbreaking scientific demonstrations [1–8]. The common denominator in these discoveries resulting from light–matter interactions is the development of intense THz pulse sources [9]. Among the various methods for generating THz pulses, the tilted-pulse front pumping (TPFP) scheme in lithium niobate (LN) is a recognized method for producing single-cycle THz pulses with high intensity [10,11]; it is the subject of ongoing intense research activity, with new developments reported every year [12–24]. Due to its very large second-order nonlinear coefficient [11] and high energy damage threshold [25], LN is the material of choice for laser pumping pulse energies beyond tens of millijoules [15,16,18,21,23,24]. Thanks to ultraintense femtosecond (fs) lasers, some of the highest THz pulse energies reported to date have reached 0.125 mJ [16], 0.2 mJ [21], 0.4 mJ [18], and 1.4 mJ [23] for an optical pump energy of 45 mJ, 70 mJ, 58 mJ, and 214 mJ, respectively. Importantly, these THz sources are very intense, but not necessarily of high average power due to the low repetition rate of the pump laser.

In parallel with these developments of high-intensity THz pulse sources, a new trend is beginning to emerge in the literature: sources with high average output power capability [26–28]. Recently, results have shown THz pulse sources with average powers up to 66 mW [26] and 144 mW [27]. The demonstrations in the present work coincide with the rise of ytterbium (Yb) lasers as a promising replacement for Ti:sapphire lasers for THz generation. Compared to the Ti:sapphire laser, the Yb laser maintains a higher average power in its regenerative amplification section [29], thus providing high repetition rate output laser pulses. The main disadvantage of this type of laser is the pulse width involved, which is longer than that obtained with Ti:sapphire lasers. Note, however, that this can be advantageous for THz generation using the LN crystal [17]. Nevertheless, pumping LN material with very high average power lasers introduces new challenges, such as heat dissipation in the LN crystal [27]. To date, for these high repetition rate sources, only low energy conversion efficiencies below 0.1% and moderate peak THz fields of <150 kV/cm have been reported [26–28]. Ideally, two characteristics must be present simultaneously: high intensity, to access nonlinear light–matter interactions or high source brightness, and high average power, to allow the sensitive detection of observed phenomena.

In this work, we report on an intense THz pulse source with 400 kV/cm at focus, with an average power of 74 mW. Instead of using a grating to perform the TPFP method [10], we used an echelon mirror, which is comparably very easy to implement. Theoretical predictions have emphasized the advantages of using a segmented TFTP beam over gratings for achieving longer interaction length [30–33]. So far, a TFTP configuration using an echelon mirror has only been demonstrated using an ultrashort (<100 fs) pump pulse [20] and a low-power, low-intensity pump beam using a digital micromirror device [34],

but without achieving a better performance than the TPFP scheme using a grating. The high performance reported in this work with a near-optimal room temperature conversion efficiency of 1.3% capitalizes on a long Fourier-limited pump pulse duration, as experimentally anticipated [17], and the long interaction length of the optical rectification (OR) process in the LN crystal, as theoretically predicted when the tilted pulse front is obtained from an echelon mirror [30]. These results were demonstrated through a novel probe pulse compression technique using only 1 μJ from the fundamental beam at a 1.0 μm wavelength. In the process, an ultrashort 512 nm probe pulse with a duration of 75 fs is obtained by first broadening the spectrum by self-phase modulation (SPM) in a pair of cadmium sulfide (CdS) crystals and using the second harmonic in a beta barium borate (BBO) crystal to spatially filter the different modes generated by the broadening process in the CdS [35] crystal. Our results represent unmatched combined characteristics with pump beam energy as low as 227 μJ.

2. EXPERIMENTAL SETUP

A. Generation Section

Figure 1 shows the experimental setup used to demonstrate this high intensity and powerful THz generation using an Yb solid-state amplified laser (model Pharos: PH1-10W from Light Conversion). This industrial laser is affordable as compared to the millijoule range amplified laser systems typically used for intense and powerful THz pulse generation [15,16,18,21–23]. Its central wavelength is 1.024 μm, with a bandwidth of 6.1 nm, for a pulse duration of 280 fs. The maximum energy is 400 μJ, with a repetition rate of 25 kHz at an average laser power of 10 W. The repetition rate can be adjusted from 25 to 200 kHz while maintaining a maximum optical output power of 10 W. In our configuration, a beam splitter ensures a 95% reflection for the pump beam and a 5% transmission for the probe beam. The pump beam is sent directly perpendicular to the surface of a Stavax, Ni-P stepped mirror (from Sodick F. T. Co.) with an aperture of 20 mm × 20 mm. The echelon mirror has the following step size: width of 187 μm and height of 85 μm. The image of the echelon mirror on the LN crystal is obtained with an achromatic cylindrical lens of 100 mm focal length in the x direction. The generator crystal is made of stoichiometric LN with a ∼1% MgO doping concentration and consists of a prism shape cut at an angle of 63°. In order to satisfy the phase-matching condition between the pump pulse and the emitted THz pulse, the tilt image from the echelon mirror is demagnified by a factor of ∼5. This demagnification factor was calculated using Eq. (1) in Ref. [20]. The emitted THz radiation is collected 84 mm away from the LN crystal by an off-axis ellipsoidal mirror (OAEM) (12-498 from Edmund Optics) of 65°, 33 mm focal length, and 31.75 mm square aperture. It is then collimated and refocused onto the electro-optical detector crystal using a pair of 50 mm diameter gold-coated off-axis parabolic mirrors (OAPMs) with focal length of 100 and 50 mm, respectively. This configuration increases the THz beam diameter by a factor of 3.1 and thus increases the focusing capability at the detection position.

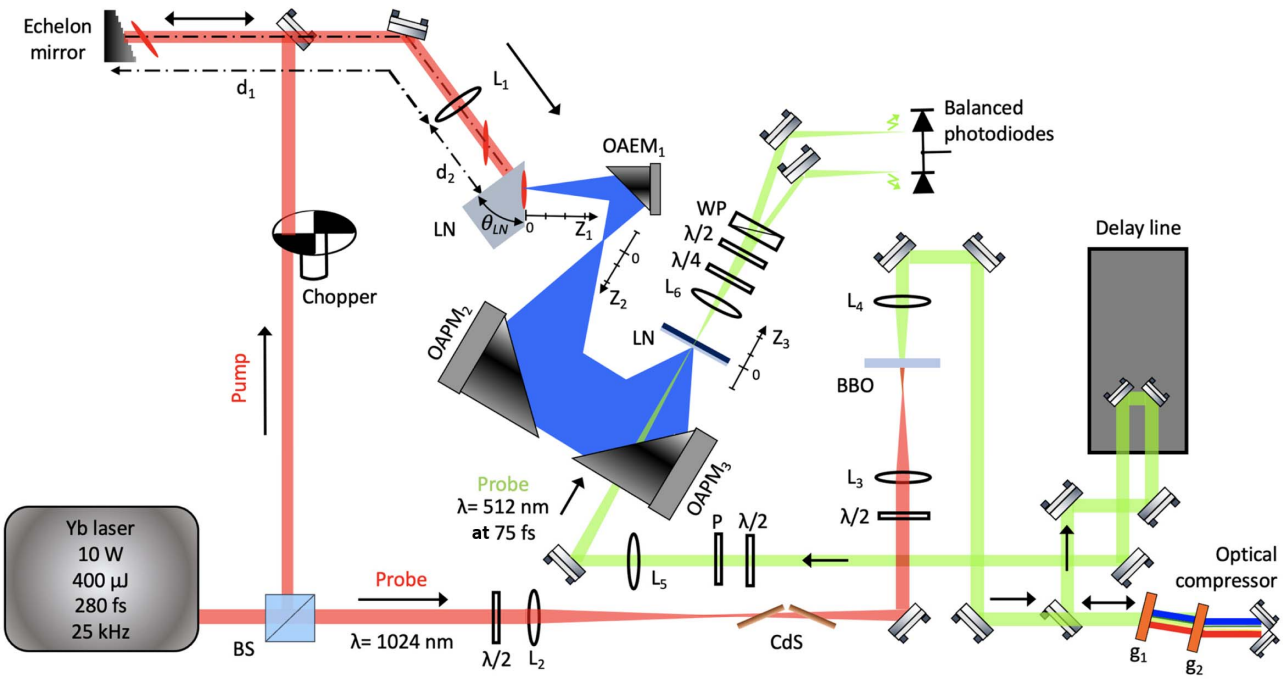

Fig. 1. Experimental setup for the generation and detection of THz pulses with the LN and their detection by EO sampling. BS, beam splitter; M_1, plane mirror reflecting the pump beam to the stair-step echelon mirror. The beam reflected by the echelon passes over M_1; d_1, 550 mm; d_2, 125 mm; θ_{LN}, LN cut angle of 63°; L_1, 100 mm focal length lens; L_2, 300 mm focal length lens; L_3, 50 mm focal length lens; L_4, 75 mm focal length lens; L_5, 100 mm focal length lens; L_6, 150 mm focal length lens; $OAEM_1$, OAEM with 83.82 mm image distance and 33.02 mm object distance; $OAPM_2$, 100 mm reflected focal length off-axis parabolic mirror; $OAPM_3$, 50 mm reflected focal length off-axis parabolic mirror; g_1 and g_2, transmissive diffracting gratings with 300 grooves/mm; $\lambda/2$, half-wave plate; $\lambda/4$, quarter-wave plate; WP, Wollaston prism; P, polarizer.

B. Detection Section

The detection of THz pulses was conducted by electro-optic (EO) sampling [36] in a 19 μm thick x-cut LN crystal deposited on a 1 mm thick z-cut LN substrate (fabricated by NanoLN). This detector has some advantages: (i) being very thin, the active layer allows detection over a wide range of frequencies without the problem of phase matching between the optical probe and the THz wave [37]; (ii) the substrate delays the first echo of the THz pulses by more than 40 ps, thus allowing an increase in the spectral resolution; and (iii) when working with intense THz pulses, a thin crystal reduces the overall modulation of the EO effect, which allows one to operate in a linear response range without the use of an attenuation filter such as high-resistivity silicon wafers. To optimally detect the electric field of a THz wave by EO sampling, it is essential to work with probe pulses of about 100 fs or less [38]. Therefore, the Pharos laser pulse duration of 280 fs is too long to effectively detect our OR-generated THz pulses and must be compressed. To this end, we used an original laser pulse compression technique, as detailed in Ref. [35]. This method requires only a microjoule or less of probe energy at the fundamental wavelength of the laser, i.e., at 1.024 μm. This laser compression method consists of three distinct steps: (i) pulse spectrum broadening by SPM, (ii) spatial and spectral filtering in a thin nonlinear crystal by second-harmonic generation, and (iii) laser pulse compression using a pair of transmission gratings. For spectral broadening by SPM, the P-polarized probe pulse is focused onto a pair of 1 mm thick CdS crystals placed at Brewster's angle with opposite orientation (see the schematic in Fig. 1). In our case, the spectrum of the probe pulse at full width at half-maximum (FWHM), after the CdS crystals, is broadened from 6.1 to 22 nm. Then, the probe beam is focused onto a 100 μm thick Type I BBO crystal to generate the second harmonic at a wavelength of 512 nm. The BBO crystal has two main functions, namely, to spatially filter the probe beam by adjusting the position of the BBO crystal with respect to the focus of the optical beam, and to select a wide and uniform spectral range. The probe pulse is finally compressed using a pair of standard transmissive gratings (GT25-03 from Thorlabs), which are also used as a geometrical filter of the remaining fundamental beam. It is worth mentioning that the use of an optical probe at the 512 nm wavelength significantly improves the dynamic range of detection, since the detected electric field is inversely proportional to the wavelength [36].

Figure 2 shows the spectral amplitude and spectral phase of the probe pulse measured using a frequency-resolved optical gating (FROG) pulse analyzer [Fig. 2(a)], and the temporal intensity and temporal phase of the compressed pulse after transmission through the gratings [Fig. 2(b)]. The spectral bandwidth of the probe beam at FWHM is 6 nm and the duration at FWHM is 75 fs. We also observe that the spectral and temporal phases are almost flat, and the temporal intensity profile of the pulse is Gaussian (i.e., without pedestal), demonstrating the good performance of our probe pulse compression chain.

C. Pump Beam Characteristics

One key feature of the TPFP technique for THz pulse generation is that it correctly images, on the LN crystal, the optical element that tilts the pulse wavefront. Ideally, the greater the interaction in the nonlinear material, the more efficient the OR process will be. Nevertheless, this is only true if the pulse retains its spatial and temporal properties. Unfortunately, it has long been known that when using a diffraction grating, the pulse duration degrades as we move away from the image plane, due to angular dispersion [39], and that the image of the tilted pulse front is imperfect due to the tilted geometry inherent in this imaging scheme [20]. To mitigate these problems, the use of a stair-step mirror has been proposed [20]. This generates beamlets whose spot size w_0 in the image plane is large, as compared to the pump pulse wavelength λ. Moreover, the Rayleigh range $z_R = \pi w_0^2 \lambda^{-1}$ remains independent of the pulse duration. Thus, beamlets can propagate over a long distance $2z_R$ without appreciable divergence. To demonstrate this point, we capture the image of the pump beam at different positions along the pump propagation direction with a CCD camera (where the position at 0 mm is the position at the center of the LN crystal). In Figs. 3(a)–3(c), we can clearly observe the image of the stepped mirror, which is sharp over a distance of 2 mm. At the 0 mm position, the dimension of the beam is 0.5 mm FWHM along the x direction [Fig. 3(d)] and 1.9 mm FWHM along the y direction. At the maximum pumping energy (227 μJ), the fluence is 34 mJ/cm^2, which is more than 20 times below the damage threshold of LN [25]. Furthermore, from the pump

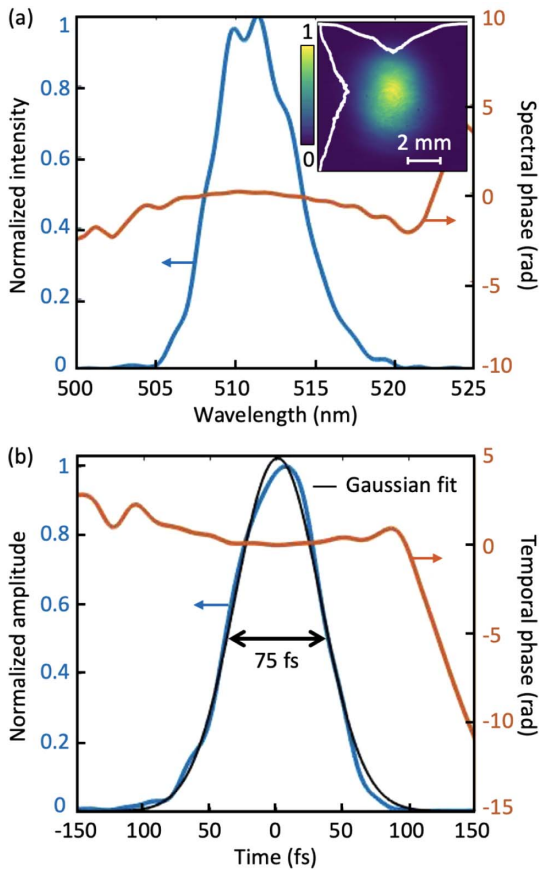

Fig. 2. Measured characteristics of the probe pulse after temporal compression. (a) Spectral amplitude and spectral phase distribution with the image of the probe spot in the inset; (b) temporal intensity and temporal phase distribution.

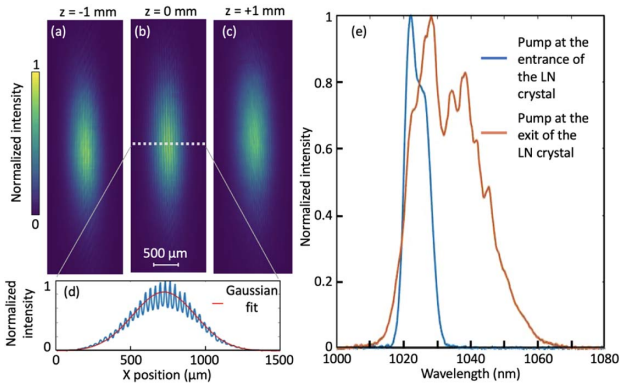

Fig. 3. Pump spot image. (a) 1 mm before the image plan position; (b) at the image plan position; and (c) 1 mm after the image plan position; (d) horizontal profile of the pump spot at the focus position; (e) normalized pump spectra at the entrance and the exit of the LN crystal after OR process.

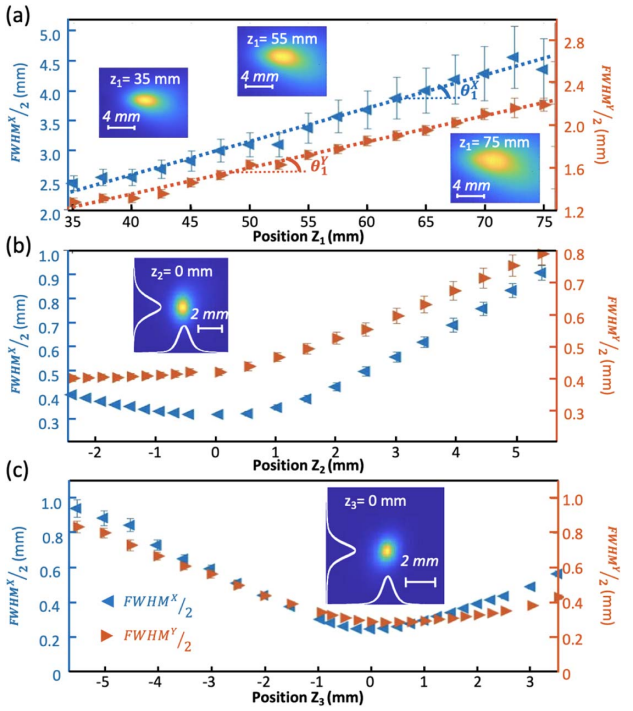

Fig. 4. THz beam radius at several locations along its propagation path (a) at the LN crystal exit facet; (b) along the focus of the OAEM; (c) along the focus of the third off-axis mirror, which corresponds to the positions Z_1, Z_2, and Z_3 in Fig. 1, respectively.

beam profiles along the z direction, we deduce a beam divergence of ∼1°. Thus, THz generation is possible over a large portion of the LN due to the large effective interaction length, with the slightly varying wavefront tilt angle allowing for efficient and optimal THz generation [20,30]. Furthermore, to validate the efficiency of the OR process, we measured the spectrum of the laser beam before and after the LN crystal [see Fig. 3(e)], and observed a significant redshift of the spectrum for the maximum energy of the pump optical pulse (at 227 µJ). This shift enables a cascade effect of optical and THz photons [40]. Thus, one pump photon participates in the generation of several THz photons, which should broaden the generated THz bandwidth.

3. RESULTS

First, we studied the variation of the THz beam size at several positions along its propagation path (positions Z_1, Z_2, and Z_3 in Fig. 1) using a THz camera (model MICROXCAM-384i, manufactured by INO). Figure 4 shows the variation of the THz beam radius along this path in the x and y directions. Figure 4(a) represents the variation of the THz spot size at the output of the LN with which we deduced the divergence of the generated THz beam. The latter is equal to 3.2° along the x direction and 1.4° along the y direction. To efficiently collect this weakly divergent source point, we prioritized the use of an ellipsoidal mirror that simultaneously captures and demagnifies an object by a factor of 2.5× thanks to its dual focal points. Figure 4(b) obtained at the focus of the OAEM ($Z_2 = 0$) confirms that a reduced THz spot image is obtained with dimensions at FWHM of 620 µm in the x direction and 830 µm in the y direction. In Fig. 4(c), the dimensions of the THz spot at the focus of the third OAPM ($Z_3 = 0$) are 490 µm in the x direction and 580 µm in the y direction at FWHM. Remarkably, the profile is Gaussian, with no sign of significant ellipticity, and is close to the diffraction limit.

The generated THz power was measured using a calibrated pyroelectric detector from GentecEO (THZ5I-BL-BNC) at the focal point of the OAEM (position Z_1 in Fig. 1) and in a purged environment. We added five high-resistivity silicon wafers and one undoped germanium wafer to avoid detector saturation. According to the transmission factors of the six filters, and taking into account the multiple-echoes from the filters, we measured a maximum THz power of 74 mW for an equivalent energy of 3 µJ per pulse. This measurement was obtained for a pumping energy of 227 µJ. This THz output energy corresponds to an optical-THz efficiency of 1.3%. Finally, taking into account the THz spot size, the pulse duration (estimated at 0.85 ps), the THz energy, and considering the losses after the following two OAPMs, we calculated a peak intensity equal to ∼1.1 GW/cm^2.

Figure 5 shows the measured time trace of the THz waveform in an unpurged environment, with a purged environment in the inset [Fig. 5(a)], and the associated unpurged spectrum in amplitude at a linear scale, with a logarithmic scale in the inset [Fig. 5(b)]. The THz waveform is single-cycle, and we can clearly distinguish ringing due to water absorption. Note that the scan range is 43 ps after the main pulse with a time step of 53 fs, and that at this stage, there still is no echo of the THz pulse observed, owing to the 1 mm LN substrate. In the frequency domain, the maximum amplitude is located at 0.9 THz over a range covering frequencies from 0.1 to 4 THz. Interestingly, the frequency bandwidth at FWHM covers a range of 0.5–1.7 THz, with a spectral resolution of 18 GHz. This is, to our knowledge, one of the largest THz bandwidths ever reported for a source of intense THz pulses from TPFP in an LN crystal at room temperature.

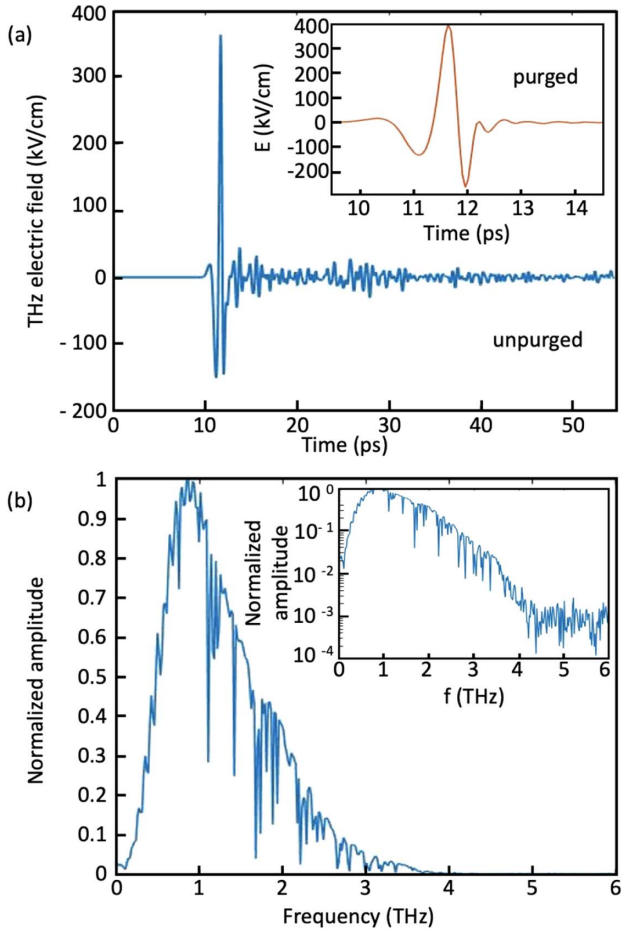

Fig. 5. (a) Temporal evolution of the generated THz pulse detected by EO sampling in an unpurged environment, with the zoom view of the temporal evolution of the THz pulse in a purged environment in the inset; (b) normalized spectrum of the generated THz pulse in an unpurged environment, with the normalized spectrum at logarithmic scale in the inset.

This demonstration is in good agreement with a scaling of the result presented in Ref. [38] and confirms the importance of the cascade effect during the OR process [40].

To fully characterize the source, we evaluate the THz electric field with a purged environment from the EO measurements by using the modulation (M) on the photodiodes, which is equal to 27.5%. The THz electric field is given by the following relation [41]:

$$E^{\mathrm{THz}} = \left| \frac{M\lambda_{\mathrm{probe}}}{2\pi t d \Gamma} \right|, \tag{1}$$

where λ_{probe} is the central wavelength of the laser beam (512 nm); $t = 0.27$ is the transmission coefficient in amplitude of the THz beam at the air–LN interface; and d is the thickness of the LN used as the THz detector. The phase retardation Γ affecting the probe beam inside the detector depends on the polarization of the THz and laser probe beams with the associated electro-optical coefficients, given by [42]

$$\Gamma = \frac{1}{2\sqrt{2}}[n_0^3(-r_{22} + r_{33}) - n_e^3 r_{33}], \tag{2}$$

where the ordinary refractive index $n_0 = 2.33$ at 0.5 μm; the extraordinary index $n_e = 2.24$ at 0.5 μm [43]; and the EO coefficients are $r_{22} = 3.4\ \mathrm{pm\,V^{-1}}$, $r_{13} = 6.5\ \mathrm{pm\,V^{-1}}$, and $r_{33} = 30.8\ \mathrm{pm\,V^{-1}}$ [42]. Therefore, by neglecting the natural birefringence of LN, a peak electric field of about 400 kV/cm was estimated.

For comparison, the THz peak electric field can also be estimated from its energy (W_{THz}), the pulse duration (τ), and the THz spot area (A) by using the following equation [41]:

$$E^{\mathrm{THz}} = \sqrt{\frac{2\eta_0 W_{\mathrm{THz}}}{\tau A}}, \tag{3}$$

where η_0 is the impedance of free space. With this method, we estimate a value of ~1 MV/cm, considering a pulse duration of 0.85 ps, a THz pulse energy of 3 μJ, and a THz spot size of 0.22 $\mathrm{mm^2}$. This method is widely used for the characterization of intense THz sources [23,24,44]. Nevertheless, it easily overestimates the actual performance. This may be due to the multiple error factors at play when estimating the energy, pulse duration, and real area of the THz beam. Therefore, we only considered the lowest evaluation obtained with the method based on the EO modulation of the signal, that is, 400 kV/cm at the peak.

Finally, to ensure the exactitude of the magnitude of the peak electric field of our source, we performed a nonlinear THz experiment with a 500 nm thick n-doped InGaAs crystal (with a carrier density of $2 \times 10^{18}\ \mathrm{cm^{-3}}$) deposited on a semi-insulating InP substrate [45–47]. The open aperture Z-scan experiment performed consists in measuring the THz transmission through the InGaAs as a function of its relative position with respect to the THz focal point in an unpurged environment and with an electric field of 310 kV/cm. The transmitted

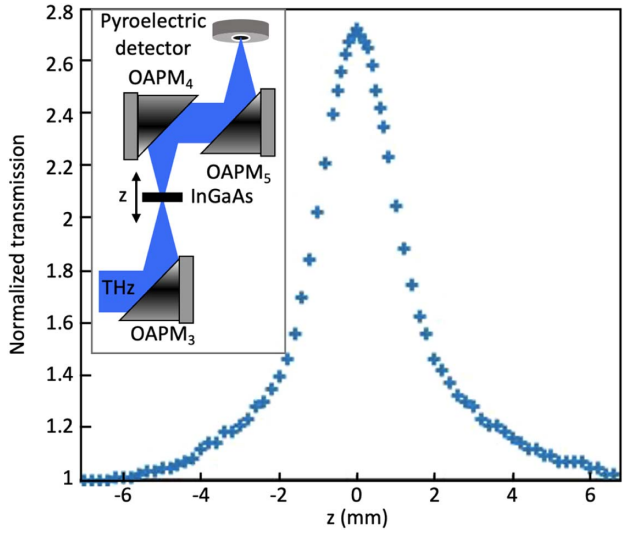

Fig. 6. Normalized THz transmission through the InGaAs sample as a function of z position, similar to Ref. [43]. Inset, experimental setup for the Z-scan measurement with InGaAs sample: $\mathrm{OAPM_3}$ of 50 mm reflected focal length; $\mathrm{OAPM_4}$ of 50 mm reflected focal length; $\mathrm{OAPM_5}$ of 100 mm reflected focal length.

Table 1. Summary of the Performances of Some of the Recent LN Sources Based on a TPFP Configuration[a]

	Output Pump Laser Parameters					Output Characteristics of the Generated THz Pulses			
Refs.	λ_0 (nm)	τ_0 (fs)	PRF (kHz)	W^L (mJ)	P^L (W)	W^{THz} (μJ)	P^{THz} (mW)	η^{THz} (%)	E^{THz} (kV/cm)
Hirori *et al.* (2011) [14]	780	85	1	4	4	3	3	0.1	1200
Fülop *et al.* (2014) [18]	1030	785	0.01	200	2	436	4	0.77	650
Ofori-Okai *et al.* (2016) [20]	800	70	1	1.5	1.5	2.1	2.1	0.21	375
Meyer *et al.* (2020) [25]	1030	550	13300	0.009	123	0.005	66	0.056	16.7
Kramer *et al.* (2020) [26]	1030	70	100	7	700	1.44	144	0.042	150
Zhang *et al.* (2021) [22]*	800	30	0.01	500	5	1400	14	0.7	6300
This work	1024	280	25	0.4	10	3.0	74	1.3	400

[a]λ_0, laser central wavelength; τ_0, laser pulse duration; PFR, laser pulse frequency rate; W^L, laser energy; P^L, average laser power; W^{THz}, THz energy; P^{THz}, average THz power; η^{THz}, optical-to-THz conversion efficiency; E^{THz}, electric field strength at the THz peak position; *, cryogenic cooling of the LN.

THz power is measured with a pyroelectric detector. Figure 6 shows the normalized nonlinear transmission as a function of the sample position relative to the focal point, with the inset showing the experimental setup. A maximum transmission enhancement factor of 2.7 is obtained at the focus. This value exceeds that reported in the past with the use of a 230 kV/cm THz pulse [47], indicating that our THz electric field evaluation is reasonable.

4. CONCLUDING REMARKS

In summary, we have demonstrated a new intense and powerful THz source that is highly scalable using a 10 W industrial fs laser. Along with this demonstration, we introduced a new pulse compression technique that is compatible with the use of a long Fourier-limited pump pulse duration for efficient THz wave generation. Using less than 1 μJ of probe pulse energy in a simple pulse compression scheme, the THz electric field can be measured with a 75 fs probe beam.

In order to appreciate these combined achievements, we summarize in Table 1 some of the most recent intense THz sources that have been reported to date using the TPFP method in an LN crystal, along with their main characteristics. Compared to Ref. [26], our source requires 70 times less input laser power to obtain just under twice their average THz power. More importantly, with 17 times less input energy per pump pulse, we obtained more than twice as much THz intensity, thanks to our record THz conversion efficiency of 1.3% in the LN at room temperature. Finally, with the use of this highly efficient and accessible system, our demonstration clearly opens the door to high repetition rate nonlinear THz science as well as to a wide range of applications outside the field of ultrafast nonlinear spectroscopy (e.g., those requiring high brightness at a high repetition rate).

Funding. Canada Research Chairs (2019-127); Natural Sciences and Engineering Research Council of Canada (2016-05020).

Disclosures. The authors declare no conflicts of interests.

Data Availability. Data underlying the results presented in this paper are not publicly available at this time but may be obtained from the authors upon reasonable request.

REFERENCES

1. H. Y. Hwang, S. Fleischer, N. C. Brandt, B. G. Perkins, M. Liu, K. Fan, A. Sternbach, X. Zhang, R. D. Averitt, and K. A. Nelson, "A review of non-linear terahertz spectroscopy with ultrashort tabletop-laser pulses," J. Mod. Opt. **62**, 1447–1479 (2015).
2. H. A. Hafez, X. Chai, A. Ibrahim, S. Mondal, D. Férachou, X. Ropagnol, and T. Ozaki, "Intense terahertz radiation and their applications," J. Opt. **18**, 093004 (2016).
3. D. Zhang, A. Fallahi, M. Hemmer, X. Wu, M. Fakhari, Y. Hua, H. Cankaya, A.-L. Calendron, L. E. Zapata, N. H. Matlis, and F. X. Kärtner, "Segmented terahertz electron accelerator and manipulator (STEAM)," Nat. Photonics **12**, 336–342 (2018).
4. D. Matte, N. Chamanara, L. Gingras, L. P. R. de Cotret, T. L. Britt, B. J. Siwick, and D. G. Cooke, "Extreme lightwave electron field emission from a nanotip," Phys. Rev. Res. **3**, 013137 (2021).
5. T. Arikawa, T. Hiraoka, S. Morimoto, F. Blanchard, S. Tani, T. Tanaka, K. Sakai, H. Kitajima, K. Sasaki, and K. Tanaka, "Transfer of orbital angular momentum of light to plasmonic excitations in metamaterials," Sci. Adv. **6**, eaay1977 (2020).
6. M. Liu, H. Y. Hwang, H. Tao, A. C. Strikwerda, K. Fan, G. R. Keiser, A. J. Sternbach, K. G. West, S. Kittiwatanakul, J. Lu, S. A. Wolf, F. G. Omenetto, X. Zhang, K. A. Nelson, and R. D. Averitt, "Terahertz-field-induced insulator-to-metal transition in vanadium dioxide metamaterial," Nature **487**, 345–348 (2012).
7. X. Li, T. Qiu, J. Zhang, E. Baldini, J. Lu, A. M. Rappe, and K. A. Nelson, "Terahertz field-induced ferroelectricity in quantum paraelectric $SrTiO_3$," Science **364**, 1079–1082 (2019).
8. H. A. Hafez, S. Kovalev, J.-C. Deinert, Z. Mics, B. Green, N. Awari, M. Chen, S. Germanskiy, U. Lehnert, J. Teichert, Z. Wang, K.-J. Tielrooij, Z. Liu, Z. Chen, A. Narita, K. Müllen, M. Bonn, M. Gensch, and D. Turchinovich, "Extremely efficient terahertz high-harmonic generation in graphene by hot Dirac fermions," Nature **561**, 507–511 (2018).
9. J. A. Fülöp, S. Tzortzakis, and T. Kampfrath, "Laser-driven strong-field terahertz sources," Adv. Opt. Mater. **8**, 1900681 (2020).
10. J. Hebling, G. Almasi, I. Z. Kozma, and J. Kuhl, "Velocity matching by pulse front tilting for large-area THz-pulse generation," Opt. Express **10**, 1161–1166 (2002).
11. J. Hebling, K.-L. Yeh, M. C. Hoffmann, B. Bartal, and K. A. Nelson, "Generation of high-power terahertz pulses by tilted-pulse-front excitation and their application possibilities," J. Opt. Soc. Am. B **25**, B6–B19 (2008).
12. K.-L. Yeh, M. C. Hoffmann, J. Hebling, and K. A. Nelson, "Generation of 10 mJ ultrashort terahertz pulses by optical rectification," App. Phys. Lett. **90**, 171121 (2007).
13. M. C. Hoffmann, K.-L. Yeh, J. Hebling, and K. A. Nelson, "Efficient terahertz generation by optical rectification at 1035 nm," Opt. Express **15**, 11706–11713 (2007).
14. H. Hirori, A. Doi, F. Blanchard, and K. Tanaka, "Single-cycle terahertz pulses with amplitudes exceeding 1 MV/cm generated by optical rectification in $LiNbO_3$," Appl. Phys. Lett. **98**, 091106 (2011).
15. J. A. Fülöp, L. Pálfalvi, M. C. Hoffmann, and J. Hebling, "Towards generation of mJ-level ultrashort THz pulses by optical rectification," Opt. Express **19**, 15090–15097 (2011).

16. J. A. Fülop, L. Palfalvi, S. Klingebiel, G. Almasi, F. Krausz, S. Karsch, and J. Hebling, "Generation of sub-mJ terahertz pulses by optical rectification," Opt. Lett. **37**, 557–559 (2012).
17. F. Blanchard, X. Ropagnol, H. Hafez, H. Razavipour, M. Bolduc, R. Morandotti, T. Ozaki, and D. G. Cooke, "Effect of extreme pump pulse reshaping on intense terahertz emission in lithium niobate at multimilliJoule pump energies," Opt. Lett. **39**, 4333–4336 (2014).
18. J.-A. Fülop, Z. Olimann, C. Lombosi, C. Skrobol, S. Klingebiel, L. Palfalvi, F. Krausz, S. Karsch, and J. Hebling, "Efficient generation of THz pulses with 0.4 mJ energy," Opt. Express **22**, 20155–20163 (2014).
19. W. R. Huang, S.-W. Huang, E. Granados, K. Ravi, K.-H. Hong, L. E. Zapata, and F. X. Kärtner, "Highly efficient terahertz pulse generation by optical rectification in stoichiometric and cryo-cooled congruent lithium niobate," J. Mod. Opt. **62**, 1486–1493 (2015).
20. B. K. Ofori-Okai, P. Sivarajah, W. Ronny Huang, and K. A. Nelson, "THz generation using a reflective stair-step echelon," Opt. Express **24**, 5057–5068 (2016).
21. X.-J. Wu, J.-L. Ma, B.-L. Zhang, S.-S. Chai, Z.-J. Fang, C.-Y. Xia, D.-Y. Kong, J.-G. Wang, H. Liu, C.-Q. Zhu, X. Wang, C.-J. Ruan, and Y.-T. Li, "Highly efficient generation of 0.2 mJ terahertz pulses in lithium niobate at room temperature with sub-50 fs chirped Ti:sapphire laser pulses," Opt. Express **26**, 7107–7116 (2018).
22. P. S. Nugraha, G. Krizsán, C. Lombosi, L. Pálfalvi, G. Tóth, G. Almási, J. A. Fülöp, and J. Hebling, "Demonstration of a tilted-pulse-front pumped plane-parallel slab terahertz source," Opt. Lett. **44**, 1023–1026 (2019).
23. B. Zhang, Z. Ma, J. Ma, X. Wu, C. Ouyang, D. Kong, T. Hong, X. Wang, P. Yang, L. Chen, Y. Li, and J. Zhang, "1.4-mJ high energy terahertz radiation from lithium niobates," Laser Photon. Rev. **15**, 2000295 (2021).
24. Q. Tian, H. Xu, Y. Wang, Y. Liang, Y. Tan, X. Ning, L. Yan, Y. Du, R. Li, J. Hua, W. Huang, and C. Tang, "Efficient generation of a high-field terahertz pulse train in bulk lithium niobate crystals by optical rectification," Opt. Express **29**, 9624–9634 (2021).
25. F. Bach, M. Mero, M.-H. Chou, and V. Petrov, "Laser induced damage studies of $LiNbO_3$ using 1030-nm, ultrashort pulses at 10–1000 kHz," Opt. Mater. Express **7**, 240–252 (2017).
26. F. Meyer, T. Vogel, S. Ahmed, and C. J. Saraceno, "Single-cycle, MHz repetition rate THz source with 66 mW of average power," Opt. Lett. **45**, 2494–2497 (2020).
27. P. L. Kramer, M. K. R. Windeler, K. Mecseki, E. G. Champenois, M. C. Hoffmann, and F. Tavella, "Enabling high repetition rate nonlinear THz science with a kilowatt-class sub-100 fs laser source," Opt. Express **28**, 16951–16967 (2020).
28. M. Abdo, S. Sheng, S. Rolf-Pissarczyk, L. Arnhold, J. A. J. Burgess, M. Isobe, L. Malavolti, and S. Loth, "Variable repetition rate THz source for ultrafast scanning tunneling microscopy," ACS Photon. **8**, 702–708 (2021).
29. J. Henrich, S. Butcher, and M. Arrigoni, "Ultrafast lasers: trends in femtosecond amplifiers—Ti:sapphire vs. ytterbium," Laser Focus World (February 18, 2020).
30. L. Wang, G. Toth, J. Hebling, and F. Kärtner, "Tilted-pulse-front schemes for terahertz generation," Laser Photon. Rev. **14**, 2000021 (2020).
31. Y. Avetisyan, A. Makaryan, V. Tadevosyan, and M. Tonouchi, "Design of a multistep phase mask for high-energy terahertz pulse generation by optical rectification," J. Infrared Millim. Terahertz Waves **38**, 1439–1447 (2017).
32. L. Pálfalvi, G. Tóth, L. Tokodi, Z. Márton, J. A. Fülöp, G. Almási, and J. Hebling, "Numerical investigation of a scalable setup for efficient terahertz generation using a segmented tilted-pulse-front excitation," Opt. Express **25**, 29560–29573 (2017).
33. G. Tóth, L. Pálfalvi, J. A. Fülöp, G. Krizsán, N. H. Matlis, G. Almási, and J. Hebling, "Numerical investigation of imaging-free terahertz generation setup using segmented tilted-pulse-front excitation," Opt. Express **27**, 7762–7775 (2019).
34. K. Murate, M. J. Roshtkhari, X. Ropagnol, and F. Blanchard, "Adaptive spatiotemporal optical pulse front tilt using a digital micromirror device and its terahertz application," Opt. Lett. **43**, 2090–2093 (2018).
35. J. E. Nkeck, L. Guiramand, X. Ropagnol, and F. Blanchard, "Broadening, nonlinear filtering, and compression of microjoule energy laser pulses at 1 μm wavelength," J. Opt. Soc. Am. B **38**, 2715–2720 (2021).
36. Q. Wu and X.-C. Zhang, "Ultrafast electro-optic field sensors," Appl. Phys. Lett. **68**, 1604–1606 (1996).
37. F. Blanchard, A. Doi, T. Tanaka, H. Hirori, H. Tanaka, Y. Kadoya, and K. Tanaka, "Real-time terahertz near-field microscope," Opt. Express **19**, 8277–8284 (2011).
38. M. Nagai, E. Matsubara, M. Ashida, J. Takayanagi, and H. Ohtake, "Generation and detection of THz pulses with a bandwidth extending beyond 4 THz using a subpicosecond Yb-doped fiber laser system," IEEE Trans. THz Sci. Technol. **4**, 440–446 (2014).
39. O. E. Martinez, "Pulse distortions in tilted pulse schemes for ultrashort pulses," Opt. Commun. **59**, 229–232 (1986).
40. M. Jewariya, M. Nagai, and K. Tanaka, "Enhancement of terahertz wave generation by cascaded $\chi^{(2)}$ processes in $LiNbO_3$," J. Opt. Soc. Am. B **26**, A101–A106 (2009).
41. M. Reid and R. Fedosejevs, "Quantitative comparison of THz emission from (100) InAs surfaces and GaAs large-aperture photoconductive switch at high fluences," Appl. Opt. **44**, 149–153 (2004).
42. F. Amirkhan, R. Sakata, K. Takiguchi, T. Arikawa, T. Ozaki, K. Tanaka, and F. Blanchard, "Characterization of thin-film optical properties by THz near-field imaging method," J. Opt. Soc. Am. B **36**, 2593–2601 (2019).
43. U. Schlarb and K. Betzler, "Refractive indices of lithium niobate as a function of wavelength and composition," J. Appl. Phys. **73**, 3472–3476 (1993).
44. F. Blanchard, L. Razzari, H. C. Bandulet, G. Sharma, R. Morandotti, J. C. Kieffer, T. Ozaki, M. Reid, H. F. Tiedje, H. K. Haugen, and F. A. Hegmann, "Generation of 1.5 μJ single-cycle terahertz pulses by optical rectification from a large aperture ZnTe crystal," Opt. Express **15**, 13212–13220 (2007).
45. L. Razzari, F. H. Su, G. Sharma, F. Blanchard, A. Ayesheshim, H.-C. Bandulet, R. Morandotti, J.-C. Kieffer, T. Ozaki, M. Reid, and F. A. Hegmann, "Nonlinear ultrafast modulation of the optical absorption of intense few-cycle terahertz pulses in n-doped semiconductors," Phys. Rev. B **79**, 193204 (2009).
46. F. Blanchard, D. Golde, F. H. Su, L. Razzari, G. Sharma, R. Morandotti, T. Ozaki, M. Reid, M. Kira, S. W. Koch, and F. A. Hegmann, "Effective mass anisotropy of hot electrons in nonparabolic conduction bands of n-doped InGaAs film using ultrafast terahertz pump-probe techniques," Phys. Rev. Lett. **107**, 107401 (2011).
47. A. Rovere, Y.-G. Jeong, R. Piccoli, S.-H. Lee, S.-C. Lee, O.-P. Kwon, M. Jazbinsek, R. Morandotti, and L. Razzari, "Generation of high-field terahertz pulses in an HMQ-TMS organic crystal pumped by an ytterbium laser at 1030 nm," Opt. Express **26**, 2509–2516 (2018).